analytical chemistry

ARTICLE

pubs.acs.org/ac

Toward the Early Evaluation of Therapeutic Effects: An Electrochemical Platform for Ultrasensitive Detection of Apoptotic Cells

Jing-Jing Zhang, Ting-Ting Zheng, Fang-Fang Cheng, Jian-Rong Zhang,* and Jun-Jie Zhu*

State Key Laboratory of Analytical Chemistry for Life Science, School of Chemistry and Chemical Engineering, Nanjing University, Nanjing 210093, People's Republic of China

Supporting Information

ABSTRACT: The ability for early evaluation of therapeutic effects is a significant challenge in leukemia research. To address this challenge, we developed a novel electrochemical platform for ultrasensitive and selective detection of apoptotic cells in response to therapy. In order to construct the platform, a novel three-dimensional (3-D) architecture was initially fabricated after combining nitrogen-doped carbon nanotubes and gold nanoparticles via a layer-by-layer method. The formed architecture provided an effective matrix for annexin V with high stability and bioactivity to enhance sensitivity. On the basis of the specific recognition between annexin V and phosphatidylserine on the apoptotic cell membrane, the annexin V/3-D architecture interface showed a predominant capability for apoptotic cell capture. Moreover, a lectin-based nanoprobe was designed by noncovalent assembly of concanavalin A on CdTe quantum dots (QDs)-labeled silica nanospheres with poly(allylamine hydrochloride) as a linker. This nanoprobe incorporated both the specific carbohydrate recognition and the multilabeled QDs-based signal amplification. By coupling with the QDs-based nanoprobe and electrochemical stripping analysis, the proposed sandwich-type cytosensor showed an excellent analytical performance for the ultrasensitive detection of apoptotic cells (as low as 48 cells), revealing great potential toward the early evaluation of therapeutic effects.

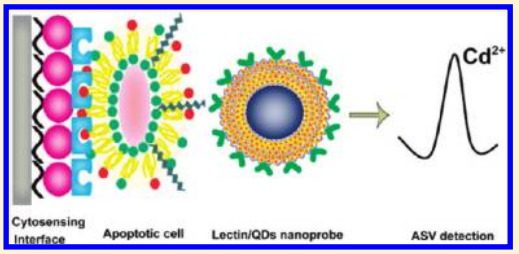

Leukemia is one of the most common fatal cancers that affects the blood and bone marrow.[1] Studies revealed that a total of 43 050 new cases and 21 840 deaths from leukemia were projected to occur in the United States in 2010.[2] Although the benefits of early diagnosis and timely intervention are well-documented, it is equally important to monitor cancer progress and patient's responses to therapy to enhance therapeutic effectiveness and prevent relapse by the patient. However, leukemia is of complicated etiology and pathogenesis, and there are a wide variety of treatment options based on the specific type of the disease and other factors.[3] Therefore, a sensitive and valuable appraisal system for early evaluation of therapeutic effects is desirable.

Apoptosis, or programmed cell death, is a highly regulated process that plays an important role in the etiology of leukemia.[4,5] At present, selective induction of apoptosis in leukemia tissue is an attractive chemotherapeutic strategy, where the extent of apoptosis and the speed of onset have been well-recognized as good prognostic indicators for the effect of therapeutic interventions.[6] For this reason, various techniques have been developed for apoptosis detection, such as electron microscopy,[7] TUNEL assay,[8] flow cytometry,[9] fluorescent sensors,[10] microfluidic devices,[11] and single-molecule spectroscopy.[12] Although these approaches have been used in some specific systems, most of them, unfortunately, either are time-consuming and labor-intensive or require highly technical expertise and relatively sophisticated instrumentation. Recently, electrochemical methods have been applied in apoptosis detection with the benefits of being simple, rapid, and convenient.[13−15] Nevertheless, these methods are still in the development phase because of the limitations of inadequate sensitivity and specificity. From this perspective, it is necessary and remains a challenge to develop feasible electrochemical biosensors with sufficient sensitivity and specificity to detect apoptosis.

Quantum dots (QDs), which exhibit sharp and well-resolved stripping voltammetric signals as the metal components, are common electroactive labels for signal amplification in electrochemical assays.[16−18] In particular, QDs can be conveniently assembled on the surface of various nanocarriers that result in multilabeled matrix to conjugate biomolecules, which dramatically enhances the intensity of the electrochemical signal and leads to ultrasensitive bioassays.[19−21] On the other hand, the chemical, physical, and functional properties of the biointerfaces are key issues in the field of electrochemical biosensors. It has been reported that nitrogen-doped carbon nanotubes (CN_X) modification can largely increase the surface area and electrical conductivity of an electrode but are limited in their solubility and biocompatibility.[22,23] In contrast, gold nanoparticles (AuNPs) have the merits of high surface reactivity and biocompatibility.[24,25] In this case, the integration of these two nanocomponents could

Received: July 14, 2011
Accepted: September 4, 2011
Published: September 04, 2011

Scheme 1. (A) Scheme of the Preparation of SiO_2@QDs−ConA Nanoprobe via Layer-by-Layer (LBL) Assembly; (B) Illustration of the Fabrication Process of the Electrochemical Cytosensing Interface; (C) Schematic Presentation of the Exposure of Phosphatidylserine Residues on the Outer Surface of the Cell Membrane during Apoptosis; (D) Sandwich Electrochemical Strategy for the Detection of Apoptotic Cells

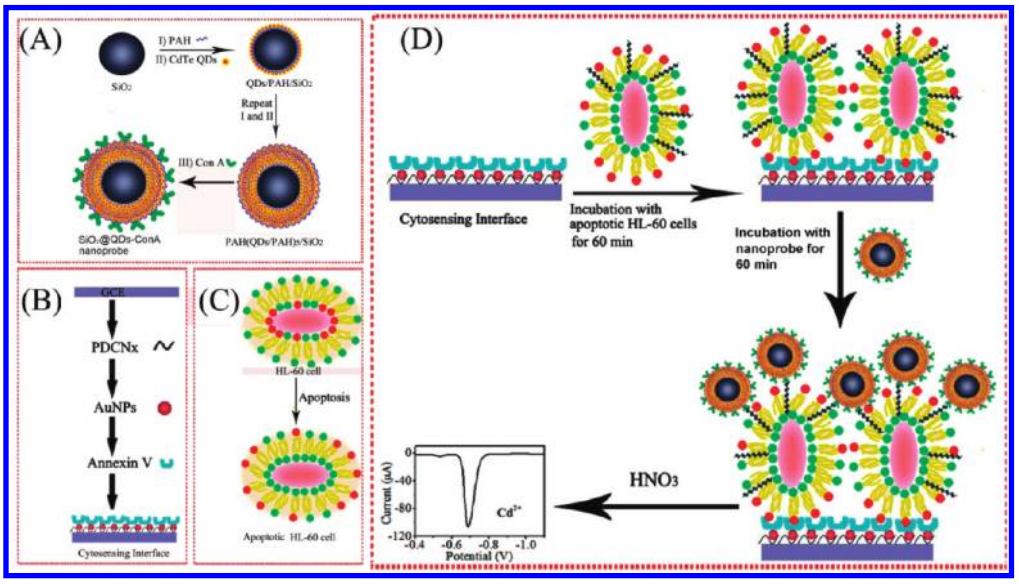

readily result in active development of a new emerging immobilization scaffold.

Herein, an electrochemical cytosensing platform was developed for apoptotic cell detection to monitor the early stages of apoptosis. To this purpose, a novel lectin-functionalized nanoprobe was first designed by noncovalent assembly of concanavalin A (ConA) on CdTe QDs-labeled silica nanospheres with poly(allylamine hydrochloride) as a linker (Scheme 1A). This nanoprobe incorporated both the specific recognition of ConA for cell-surface mannosyl groups and the electrochemical signal amplification of multilabeled SiO_2@QDs nanocomposites. Then, a three-dimensional (3-D) architecture was fabricated as the base of the cytosensor by combining CN_X and AuNPs with a layer-by-layer (LBL) method as shown in Scheme 1B. The formed architecture provided an effective matrix for the immobilization of annexin V to enable annexin V hold high stability and bioactivity, resulting in the sensitivity enhancement. After that, human leukemic HL-60 cells were chosen as a model and exposed to apoptosis inducer, which led to the translocation of phosphatidylserine (PS) from the inner side of the plasma membrane to the outer layer as shown in Scheme 1C. On the basis of the specific recognition between annexin V and PS on the apoptotic cell membrane, the annexin V/3-D architecture interface showed a predominant capability for apoptotic cell capture. By coupling with SiO_2@QDs−ConA nanoprobe and electrochemical stripping technique, a novel electrochemical platform was finally developed for the detection of apoptotic cells (Scheme 1D). This platform not only exhibited attractive performances in cytosensing but also presented a significant tool to monitor the early stages of apoptosis, suggesting potential applications toward the early evaluation of therapeutic effects.

EXPERIMENTAL SECTION

Materials and Reagents. Concanavalin A, poly(diallyldimethylammonium chloride) (PDDA, MW = 200 000−350 000), poly(allylamine hydrochloride) (PAH, MW = 15 000), bovine serum albumin (BSA), 3-mercaptopropionic acid (MPA), and 2-(*N*-morpholino)ethanesulfonic acid (MES) were purchased from Sigma-Aldrich. The silica spheres with 500 nm diameters were purchased from Alfa Aesar. Annexin V was obtained from Beijing Biosynthesis Biotechnology Co. Ltd. (Beijing, China). The apoptosis inducers kit (C0005) was purchased from Beyotime Institute of Biotechnology (Haimen, China). Human acute promyelocytic leukemia cells (HL-60) and the annexin V−FITC apoptosis detection kit were purchased from Nanjing Keygen Biotechnology Co. Ltd. (Nanjing, China).

The PDDA-functionalized CN_x ($PDCN_X$) was prepared as described in ref 26. AuNPs were prepared by a modified citrate-reduction method.[27] The AuNPs modified indium−tin oxide (ITO) electrode and MPA-capped CdTe QDs were prepared as reported previously.[28] The as-synthesized MPA−CdTe QDs have an average diameter of 4.2 ± 0.6 nm and possess a cubic zinc blende structure with good crystallinity (see Supporting Information Figure S1). Phosphate buffer saline (PBS, pH 7.4) containing 137 mM NaCl, 2.7 mM KCl, 8.7 mM Na_2HPO_4, and 1.4 mM KH_2PO_4 was used as incubation buffer. All other reagents were of analytical grade. All aqueous solutions were prepared using ultrapure water (Milli-Q, Millipore).

Apparatus. The transmission electron microscopic (TEM) image was observed under a JEM-2100 transmission electron microscope (JEOL Ltd., Japan). X-ray powder diffraction (XRD) measurements were performed on a Japan Shimadzu XRD-6000 diffractometer with Cu Kα radiation (λ = 0.15418 nm); a scanning rate of 0.05 deg/s was applied to record the patterns in the 2θ range of 10−70°. The photoluminescence spectra were recorded with a F920 fluorescence spectrometer (Edinburgh Instruments Ltd., U.K.). Scanning electron micrographs (SEM) were obtained with a Hitachi S4800 scanning electron microscope. The static water contact angles were measured at 25 °C by a contact angle meter (Rame-Hart-100) employing drops of pure deionized water. Confocal laser scanning microscopy (CLSM) studies were performed using a Leica TCS SP5 microscope (Germany) with

dx.doi.org/10.1021/ac201804b |*Anal. Chem.* 2011, 83, 7902–7909

excitation at 405 nm. Electrochemical measurements were performed on a CHI 660C workstation (Shanghai Chenhua Apparatus Corporation, China) with a conventional three-electrode system composed of a platinum wire as the auxiliary, a saturated calomel electrode as the reference, and a mercury film modified glassy carbon electrode (GCE) as the working electrode. Electrochemical impedance spectroscopy (EIS) was performed with an Autolab electrochemical analyzer (Eco Chemie, The Netherlands) in 10 mM $K_3Fe(CN)_6/K_4Fe(CN)_6$ with 1.0 M KCl as the supporting electrolyte, within the frequency range of 0.01 Hz to 100 kHz.

Preparation of the Nanoprobe. The SiO_2@QDs−ConA nanoprobe was prepared via a LBL assembly approach. Briefly, 10.0 mg of SiO_2 was dispersed into a 0.2 wt % PAH salt solution (0.02 M NaCl, 1.0 mL) and sonicated for 10 min to give a homogeneous suspension. Residual PAH polymer was removed by centrifugation (5000 rpm, 5 min), and the precipitate was washed with water for at least three times. Subsequently, the obtained positively charged PAH−SiO_2 was redispersed in 2.0 mL of negatively charged CdTe QDs solution, and the reaction mixture was sonicated for 20 min, after which the excessive QDs were removed by centrifugation and redispersed in water. This procedure was repeated (alternating between PAH and QDs) until five bilayers were deposited. For the noncovalent assembly of ConA, the SiO_2@QDs was coated with another layer of PAH to obtain a positively charged surface and then mixed with 1.0 mL of 1.0 mg mL^{-1} ConA (50 mM, pH 6.0 MES buffer). The reaction mixture was incubated 2 h at room temperature under shaking and kept overnight at 4 °C. After that, the mixture was washed with incubation buffer and centrifuged at 5000 rpm for 5 min three times, and the supernatant was discarded. The SiO_2@QDs−ConA nanoprobe was obtained by redispersing the precipitate in the incubation buffer containing 1 mM Ca^{2+}, 1 mM Mn^{2+}, and 0.1% BSA and stored at 4 °C.

Cell Culture and Induction of Apoptosis. HL-60 cells were cultured in a flask in RPMI 1640 medium (Gibco, Grand Island, NY) supplemented with 10% fetal calf serum (FCS, Sigma), penicillin (100 μg mL^{-1}), and streptomycin (100 μg mL^{-1}) in an incubator (5% CO_2, 37 °C). At the logarithmic growth phase, the cells were collected and separated from the medium by centrifugation at 1000 rpm for 5 min and then resuspended in fresh culture medium to obtain a homogeneous cell suspension with the final concentration of 5×10^5 cells mL^{-1}. Cell number was determined using a Petroff-Hausser cell counter (U.S.A.). Then, 4 mL of HL-60 cell suspension was treated with an apoptosis inducers kit (1 μL/mL) for 0, 2, 4, 8, 16, 24, 32, 48, and 72 h, respectively. After that, cells were collected, washed twice with PBS, and redispersed in the incubation buffer containing 1 mM Ca^{2+} and 1 mM Mn^{2+}. The apoptotic cell suspensions with various concentrations were prepared from this stock.

Preparation of the Cytosensor and Cell Capture. $PDCN_X$ (5.0 mg mL^{-1}, 5 μL) was first dropped on the bare GCE and dried in a silica gel desiccator and then immersed into a AuNPs solution for 1 h to obtain AuNPs/$PDCN_X$/GCE. The immobilization of annexin V was accomplished by dropping 5 μL of 5 μg mL^{-1} annexin V solution on the AuNPs/$PDCN_X$. The electrode was incubated at 4 °C for 24 h in a moisture atmosphere to avoid evaporation of solvent. Following a careful rinse with incubation buffer, the annexin V/AuNPs/$PDCN_X$/GCE was immersed in BSA (1%) solution for 1 h to block the nonspecific binding sites. After that, the electrode was soaked in 100 μL of apoptotic cell suspension at a certain concentration and incubated at 37 °C for 1 h to capture the cells via the specific binding between annexin V and cell-surface phosphatidylserine. Then the electrode was taken out and rinsed with incubation buffer to remove the noncaptured cells. The obtained HL-60/annexin V/AuNPs/$PDCN_X$/GCE was used for subsequent assays.

Electrochemical Detection of Captured QDs Nanoprobe. After the capture of apoptotic cells, the electrode was immediately incubated with 60 μL of SiO_2@QDs−ConA nanoprobe at 37 °C for 1 h. Then the electrode was washed thoroughly with incubation buffer containing 1 mM Ca^{2+} and 1 mM Mn^{2+} to remove nonspecifically bound nanoprobe to minimize the background response. Afterward, the electrode was immersed in 500 μL of 0.1 M HNO_3 solution for 2 h to dissolve the captured QDs nanoprobe, and the resulting solution was mixed with 4.5 mL of 0.2 M pH 4.6 HAc−NaAc buffer to perform anodic stripping voltammetric (ASV) detection with a mercury film modified GCE.[29] Mercury film was electrodeposited on the surface of glassy carbon electrode by four cycles of alternate deposition at −0.1 V for 40 s and scanned from −0.9 to −0.2 V in 0.2 M pH 5.2 HAc−NaAc buffer containing 40 μg mL^{-1} Hg^{2+} under N_2 atmosphere. The anodic stripping detection was carried out by electrodepositing cadmium at −1.1 V for 6 min and then stripping from −0.9 to −0.2 V under N_2 atmosphere using a square-wave voltammetric waveform, with a 4 mV potential step, a 25 Hz frequency, and an amplitude of 25 mV.

Flow Cytometric Analysis. HL-60 cells treated with an apoptosis inducers kit for different times were collected by centrifugation, washed with sterile cold PBS, and resuspended in 500 μL of binding buffer. Then, the cells were stained with annexin V−fluorescein isothiocyanate (FITC) and propidium iodide (PI) according to the manufacturer's instructions. The sample was immediately analyzed on the FACS Sort flow cytometer (Becton Dickinson, U.S.A.) and CLSM with excitation at 488 nm.

RESULTS AND DISCUSSION

Characterization of SiO_2@QDs−ConA Nanoprobe. Since the pioneering work of Decher and Hong,[30] the LBL technique has been widely used in the construction of multifunctional nanoassemblies.[31−33] We employ the technique for the construction of a novel lectin-based nanoprobe, namely, SiO_2 core particles coated with CdTe QDs/PAH multilayers and terminated with an outermost layer of ConA (Scheme 1A). Figure 1A shows the TEM image of the resulting SiO_2@QDs composite. The SiO_2@QDs displays a rather rough surface after the five-bilayers coating of CdTe QDs/PAH. Meanwhile, the high-resolution TEM (HRTEM) image in Figure 1B allows visualization of numerous, dark "QD islands" on the carrier SiO_2, and the thickness of the multilayer shell is about 16.0 nm.

The multilayer coating of QDs was further verified by CLSM. As shown in Figure 1C, the SiO_2@QDs generates a strong, homogeneous, red fluorescence, which suggests the uniform distribution of QDs on the SiO_2 surface. The CLSM image also shows that the SiO_2@QDs are well-separated in solution. Figure 1D shows the photoluminescence spectra of pure CdTe QDs and SiO_2@QDs nanocomposite. A red shift of the PL peak occurred after the formation of the QDs/PAH multilayer shell, which was possibly due to interparticle interaction in the multilayer shell. When CdTe QDs were deposited as a thin layer, the bound polymer can hold QDs closer together in the layer than in

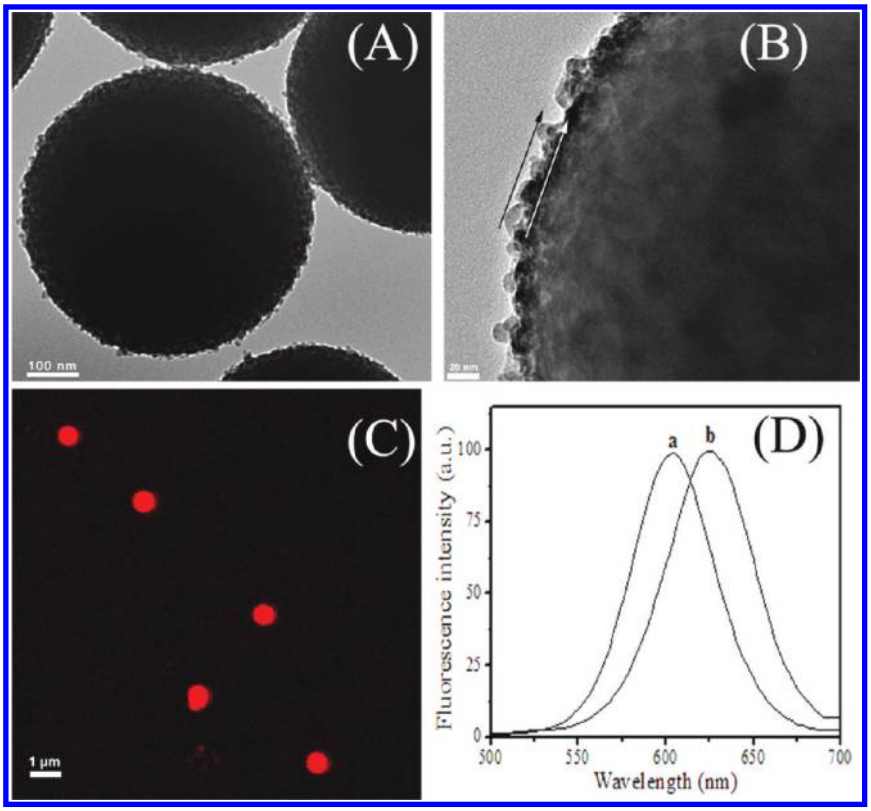

Figure 1. TEM, HRTEM, and CLSM images of the SiO_2@QDs nanocomposite with five bilayers (A−C). (D) Normalized fluorescence spectra of (a) pure CdTe QDs and (b) SiO_2@QDs nanocomposite.

suspension, which can facilitate energy transfer from small to large QDs and result in an apparent red shift.[34]

Additionally, the LBL assembly process was monitored by microelectrophoresis measurements (expressed as a *z*-potential), which is an effective method of characterizing the surface charge of colloid particles. The values of the *z*-potential of SiO_2, PAH/SiO_2, QDs/PAH/SiO_2, and ConA/PAH/$(QDs/PAH)_5/SiO_2$ are shown in Supporting Information Figure S2. The SiO_2 spheres were negatively charged at neutral pH with a *z*-potential of −37.3 mV (a in Supporting Information Figure S2A), which was due to the surface hydroxyl groups. The subsequent alternate absorption of PAH and QDs layers onto the surface yielded *z*-potentials of +19.9 mV (b in Supporting Information Figure S2A) and −25.1 mV (c in Supporting Information Figure S2A), respectively. Considering that ConA is negatively charged at neutral pH (pI ∼ 4.7),[35] an additional positively charged PAH layer was coated on the $(QDs/PAH)_5/SiO_2$. It is interesting to note that the value of the *z*-potential decreases to +1.11 mV (d in Supporting Information Figure S2A), indicating the noncovalent assembly of ConA.

Altogether, these results suggested the successful preparation of SiO_2@QDs−ConA nanoprobe. In this case, the lectin-based nanoprobe proposed for each molecular recognition event contains numerous QDs-based electrochemical species, and analytical signal output is thus expected to be dramatically amplified.

Assembly of the Electrochemical Cytometric Recognition Platform. Nitrogen-doped carbon nanotubes with defective bamboo-like structure are typically of a larger surface-active group-to-volume ratio, superb thermal stability, and good electrical and mechanical properties. As discussed in our previous report, the integration of CN_X with gold nanoparticles was beneficial to lectin loading and cell capture.[26] Herein, the AuNPs/$PDCN_X$ was assembled on the surface of a GCE for binding of annexin V to generate a cytometric recognition platform. Annexin V is a Ca^{2+}-dependent phospholipid-binding protein, which has high specific affinity for PS on the apoptotic cell membrane. The biocompatibility of the cytometric recognition platform was first characterized by hydrophilicity analysis. As shown in Supporting Information Figure S2, the contact angle of the electrode surface decreased with the stepwise assembly of $PDCN_X$ and AuNPs. This result suggested that the AuNPs/$PDCN_X$/GCE interface had a better hydrophilicity, which was in favor of enhancing protein loading and retaining the bioactivity.

The stepwise fabrication process of the cytosensing interface was also characterized by SEM (Figure 2). It can be seen that the $PDCN_X$ were mostly in the form of small bundles or single tubes on GCE (Figure 2A). In comparison with $PDCN_X$, the AuNPs/$PDCN_X$ film exhibited a 3-D architecture morphology with uniform and abundant decoration of gold nanoparticles (Figure 2B). This uniform 3-D interface provided a significant increase of effective electrode surface for loading biomolecules. After being immersed in annexin V solution for 24 h, the surface became much rougher and richer in texture (Figure 2C), due to the aggregation of annexin V. It should be noted that the incorporation of annexin V with AuNPs/$PDCN_X$ architecture could offer a nanoscale analogue of extracellular matrix for further cell capture.

The electrochemical properties of the cytometric recognition platform were further studied by monitoring the change of electron-transfer resistance of $[Fe(CN)_6]^{3-/4-}$ as redox probes with EIS. As shown in Figure 2D, the AuNPs/$PDCN_X$ showed an electron-transfer resistance of about 30.2 Ω (curve a), implying the good electrical conductivity of the interface. After being

dx.doi.org/10.1021/ac201804b |*Anal. Chem.* 2011, 83, 7902–7909

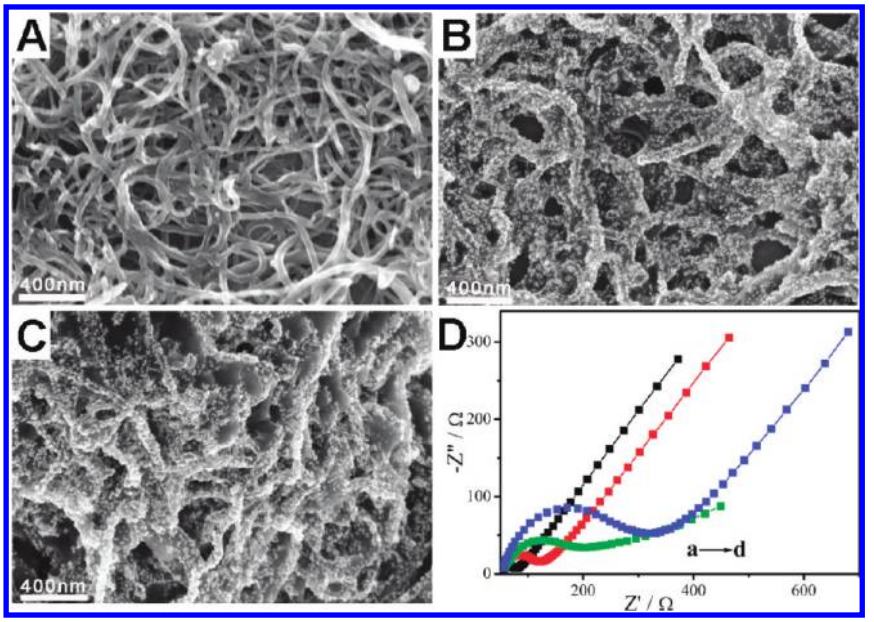

Figure 2. SEM images of $PDCN_X$/GCE (A), AuNPs/$PDCN_X$/GCE (B), and annexin V/AuNPs/$PDCN_X$/GCE (C). (D) EIS of the electrode at different fabrication stages in 10 mM $[Fe(CN)_6]^{3-/4-}$ with 1.0 M KCl: (a) AuNPs/$PDCN_X$; (b) curve a plus annexin V; (c) curve b plus apoptotic cells; (d) curve c plus SiO_2@QDs−ConA.

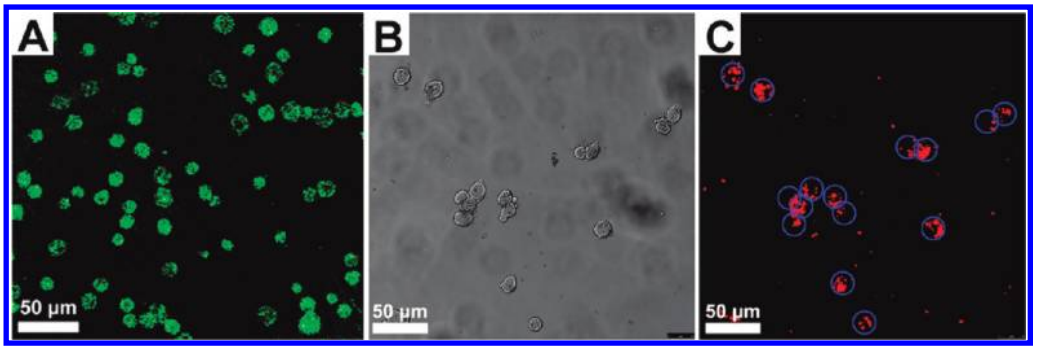

Figure 3. (A) CLSM image of apoptotic HL-60 cells stained by annexin V−FITC after incubation with apoptosis inducer for 16 h. The bright-field (B) and fluorescence (C) images of apoptotic HL-60 cells after being captured on the ITO/AuNPs/annexin V and further recognized by the SiO_2@QDs−ConA nanoprobe.

immersed in annexin V solution, the resistance increased to 73.0 Ω (curve b), suggesting that annexin V molecules were immobilized on the electrode and blocked the electron exchange between the redox probe and the electrode. The results were consistent with the observation from SEM images. Subsequently, after the capture of apoptotic cells, the resistance increased again (curve c), due to the dielectric behavior of cells for interfacial electron-transfer processes. Additionally, the access of the redox probe to the electrode could further be hindered after incubation with SiO_2@QDs−ConA nanoprobe, due to the resistance of proteins, generating an obvious increase of resistance (curve d). These results verified the successful construction of the sandwich-type electrochemical cytosensor.

Construction of the Apoptotic Cell Model. For validation of the sandwich-type electrochemical cytosensor for apoptotic cells detection, HL-60 were chosen as a model and exposed to apoptosis inducer for induction of apoptosis. Figure 3A shows the confocal image of HL-60 cells stained by annexin V−FITC after incubation with apoptosis inducer for 16 h. It is easily observed that a majority of cells emit bright green fluorescence, which resulted from the specific binding of annexin V−FITC toward phosphatidylserine (PS). However, PS is a phospholipid component, usually kept on the inner leaflet of cell membranes, but becomes exposed on the surface of the cell during apoptosis.[36,37] The staining of normal HL-60 cells with annexin V−FITC displayed relatively weak green fluorescence (see Supporting Information Figure S3). Therefore, the observation of the confocal fluorescence image indicated that the incubation of HL-60 model cells with apoptosis inducer for 16 h could remarkably result in apoptosis.

Furthermore, the CLSM experiments were performed to confirm the targeting effect of the SiO_2@QDs−ConA nanoprobe. For convenience, the ITO/AuNPs as a substrate was used to immobilize annexin V. Figure 3B shows the representative bright-field image of the ITO/AuNPs/annexin V biointerface after stepwise incubation with apoptotic cell suspension and nanoprobe. It is obvious that the biointerface ensures the effective binding between cell-surface phospholipid and annexin V on

electrodes. Meanwhile, in the corresponding fluorescence image (Figure 3C), the red fluorescence signal of QDs was clearly visible on the surface of captured cells, indicating the efficient recognition between the lectin-based QDs nanoprobe and mannosyl groups on the apoptotic cell surface. This result revealed the feasibility of detection of apoptotic cells on the sandwich-type cytometric recognition platform.

Analytical Performance of the Electrochemical Cytosensor. After the CdTe QDs were dissolved with HNO_3 from the captured SiO_2@QDs−ConA nanoprobe on the cytosensor, the dissolved cadmic component was detected by anodic stripping voltammetry (ASV). A distinct stripping voltammetric peak for the oxidation of Cd responding to the concentrations of 1×10^7 apoptotic cells mL^{-1} could be observed at around −0.7 V in 0.2 M, pH 5.2 HAc−NaAc buffer (curve c in Figure 4). In contrast, the stripping voltammograms of the cytosensor without cells (curve a) or with the same amount of normal cells (curve b) both showed low electrochemical response, which may be due to the little nonspecific adsorption of SiO_2@QDs−ConA or normal cells. As compared in the inset of Figure 4, the peak current for apoptotic cells is about 3.9- and 15.0-fold higher than that obtained with normal cells and without cells, respectively, revealing the high selectivity of the proposed approach. The resulting high selectivity could be possibly due to the highly specific bindings between annexin V and PS on the apoptotic cell membrane as well as the effective recognition by SiO_2@QDs−ConA nanoprobe.

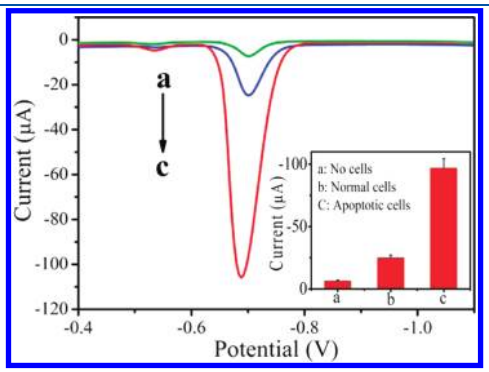

Figure 4. ASV measurements for the cytosensor without cells (a) and with normal cells (b) and apoptotic cells (c). The inset is the corresponding peak currents.

To obtain good analytical performance, some important parameters were optimized. As shown in Supporting Information Figure S4, the optimized deposition potential and accumulation time were −1.1 V and 6 min, respectively. The proposed electrochemical cytosensor was used to investigate the apoptosis process of HL-60 cells induced by apoptosis inducer. Figure 5A shows the stripping signals that were responsive to the change in incubation time of apoptosis inducer. At the early stage for 8 h, the stripping signals changed gradually at a low level, implying that a part of the HL-60 cells was induced to apoptosis that led to the exposure of PS. As the apoptosis induction proceeded to 16 h, a significant increase of peak current was observed, revealing a remarkable apoptotic state of HL-60 cells. However, the response showed a decreasing trend thereafter. Taken together, the peak currents exhibited a negative parabolic profile with a maximum at 16 h (Figure 5B), which indicated that PS externalization is a time-dependent event occurring during cell apoptosis.

To confirm the time course of PS externalization of the apoptotic cells, HL-60 cells treated with apoptosis inducer for different times were further analyzed by flow cytometry analysis with annexin V−FITC and PI double staining. As shown in Supporting Information Figure S5, the percentage of early [annexin V (+)/PI (−)] and late [annexin V (+)/PI (+)] stage

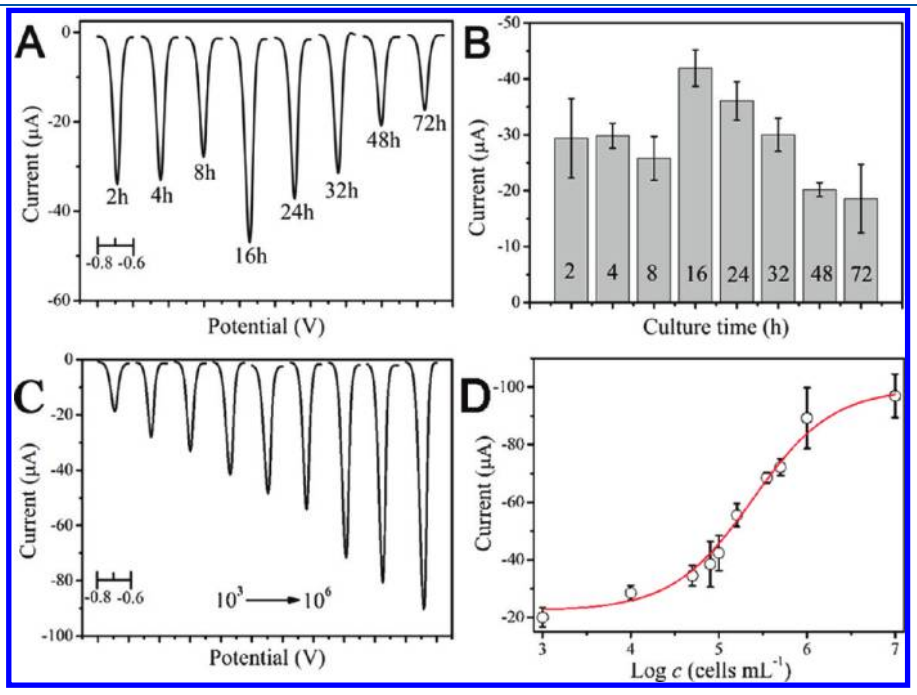

Figure 5. (A) ASV measurements for apoptotic cells after the HL-60 cells were incubated with apoptosis inducer for different times. (B) The dependence of peak currents on the incubation time of apoptosis inducer. (C) ASV measurements for different concentrations of apoptotic cells: 10^3, 10^4, 5×10^4, 8×10^4, 1×10^5, 1.6×10^5, 3.5×10^5, 5×10^5, and 1×10^6 (left to right). HL-60 cells were incubated with apoptosis inducer for 16 h. (D) Relationship between the peak currents and the cell concentration. Error bars represent one standard deviation for three independent measurements.

dx.doi.org/10.1021/ac201804b |*Anal. Chem.* 2011, 83, 7902–7909

of apoptotic cells was only about 3.02% and 3.56% in the absence of apoptosis inducer (Supporting Information Figure S5A). However, with increasing incubation time of apoptosis inducer, the percentage of apoptotic cells (both early and late stage) increased to 18.3% at 4 h (Supporting Information Figure S5B) and 48.3% at 16 h (Supporting Information Figure S5C), respectively. This result revealed a time-dependent increasing trend of cell apoptosis, which was consistent with the electrochemical results in Figure 5A. Interestingly, although the percentage of apoptotic cells at 48 h of induction further increased to 63.5% (Supporting Information Figure S5D), the corresponding stripping signal decreased as compared with 16 h of induction (Figure 5B). One possible explanation is that the stripping signal of the sandwich-type cytosensor was directly related to the amount of immobilized SiO_2@QDs−ConA nanoprobe, which not only depended on the amount of captured apoptotic cells but also was associated with the expression of carbohydrates on the cell surface. In addition, the apoptotic cells referring to 48 h of induction were mainly in the late stage (about 60.3%). In this case, cell-surface carbohydrate profiles were altered by surface glycosidase[38−40] and led to a loss of binding sites for SiO_2@QDs−ConA nanoprobe, resulting in a decreased stripping signal. In view of these findings, we might conclude that the proposed sandwich-type cytosensor can not only be used to monitor the process of apoptosis but also can provide more insight on the glycosylation alterations of cells undergoing apoptosis.

In order to truly evaluate the sensitivity of the proposed cytosensor, the dynamic range for the detection of apoptotic cells was examined with 16 h of induction as a model. Figure 5C shows the stripping signals that were responsive to the change in different concentrations of apoptotic cells. Here, the concentrations of apoptotic cells were defined as the total amount of cells used for electrode incubation after 16 h of apoptosis induction. The peak current was proportional to the logarithm value of apoptotic cell concentration over a four decade range from 1×10^3 to 1×10^7 cells mL^{-1} (Figure 5D). It should be noted that the calibration curve reached the plateau when the concentration of apoptotic cells is up to 1×10^7 cells mL^{-1}, which was due to the saturated capture of apoptotic cells on the cytosensor. The detection limit was 1×10^3 cells mL^{-1} (S/N = 3). Taking into account that 100 μL of cell suspension was used for incubation and about 48% was in the apoptotic state, the presented cytosensor achieved the limit of detection of only 48 apoptotic HL-60 cells, which was much lower than that of 2×10^5 apoptotic A549 cells at the pyrolytic graphite electrode and 10^4 apoptotic Jurkat cells at a AuNPs-modified gold electrode.[14,15] The high sensitivity achieved resulted from the combination of the dual signal amplification by the nanoprobe based on the LBL method, the enormous QDs loading, and the predominant capability for apoptotic cell capture by the annexin V/3-D architecture. In addition, compared with conventional QDs-based fluorescent assays for cancer biomarkers,[41,42] the proposed electrochemical cytosensor is not limited by the need for complicated and expensive instruments, as well as skilled technical personnel.

CONCLUSIONS

In summary, a novel lectin-functionalized SiO_2@QDs nanoassemblies was newly explored and used as an amplified signal probe for ultrasensitive detection of apoptotic cells for the first time. Several advantages of the proposed method should be highlighted. First, a large number of CdTe QDs were assembled onto the silica spheres via LBL assembly, which could greatly amplify the QDs electrochemical signals. Second, a 3-D architecture of biointerface based on $PDCN_X$−AuNPs and annexin V was employed in the cytosensor, which significantly improved the capture of apoptotic cells. Third, by coupling with QDs-based nanoprobe and electrochemical stripping analysis, the proposed sandwich-type cytosensor exhibits attractive performance for detection of apoptotic cells with broad detection range, low detection limit, and good selectivity. Such a smart platform presents a significant tool to monitor the early stages of apoptosis, suggesting potential applications toward the early evaluation of therapeutic effects.

ASSOCIATED CONTENT

Supporting Information. Additional information as noted in text. This material is available free of charge via the Internet at http://pubs.acs.org.

AUTHOR INFORMATION

Corresponding Author
*E-mail: jjzhu@nju.edu.cn (J.-J.Z.), jrzhang@nju.edu.cn (J.-R.Z.).

ACKNOWLEDGMENT

This work was financially supported by the National Natural Science Foundation of China (Nos: 20821063, 21020102038, 20975048), National Basic Research Program of China (2011-CB933502), and The Fundamental Research Funds for the Central Universities (No. 1112020504).

REFERENCES

(1) Bordignon, C. *Nature* **2006**, *441*, 1100–1102.
(2) Jemal, A.; Siegel, R.; Xu, J. Q.; Ward, E. *CA—Cancer J. Clin.* **2010**, *60*, 277–230.
(3) Chiorazzi, N.; Rai, K. R.; Ferrarini, M. *N. Engl. J. Med.* **2005**, *352*, 804–815.
(4) van Tilborg, G. A. F.; Mulder, W. J. M.; Chin, P. T. K.; Storm, G.; Reutelingsperger, C. P.; Nicolay, K.; Strijkers, G. J. *Bioconjugate Chem.* **2006**, *17*, 865–868.
(5) Martinez, M. M.; Reif, R. D.; Pappas, D. *Anal. Methods* **2010**, *2*, 996–1004.
(6) Pui, C. H.; Evans, W. E. *N. Engl. J. Med.* **2006**, *354*, 166–178.
(7) Yasuhara, S.; Zhu, Y.; Matsui, T.; Tipirneni, N.; Yasuhara, Y.; Kaneki, M.; Rosenzweig, A.; Martyn, J. A. J. *J. Histochem. Cytochem.* **2003**, *51*, 873–885.
(8) Darzynkiewicz, Z.; Galkowski, D.; Zhao, H. *Methods* **2008**, *44*, 250–254.
(9) Song, E. Q.; Wang, G. P.; Xie, H. Y.; Zhang, Z. L.; Hu, J.; Peng, J.; Wu, D. C.; Shi, Y. B.; Pang, D. W. *Clin. Chem.* **2007**, *53*, 2177–2185.
(10) Quinti, L.; Weissleder, R.; Tung, C. H. *Nano Lett.* **2006**, *6*, 488–490.
(11) Wlodkowic, D.; Faley, S.; Zagnoni, M.; Wikswo, J. P.; Cooper, J. M. *Anal. Chem.* **2009**, *81*, 5517–5523.
(12) Walter, N. G. *Biopolymers* **2007**, *85*, 103–105.
(13) Xiao, H.; Liu, L.; Meng, F. B.; Huang, J. Y.; Li, G. X. *Anal. Chem.* **2008**, *80*, 5272–5275.
(14) Liu, T.; Zhu, W.; Yang, X.; Chen, L.; Yang, R. W.; Hua, Z. C.; Li, G. X. *Anal. Chem.* **2009**, *81*, 2410–2413.
(15) Tong, C. Y.; Shi, B. X.; Xiao, X. J.; Liao, H. D.; Zheng, Y. Q.; Shen, G. L.; Tang, D. Y.; Liu, X. M. *Biosens. Bioelectron.* **2009**, *24*, 1777–1782.

(16) Baron, R.; Willner, B.; Willner, I. *Chem. Commun.* **2007**, *4*, 323–332.
(17) Du, D.; Wang, J.; Wang, L. M.; Lu, D. L.; Smith, J. N.; Timchalk, C.; Lin, Y. H. *Anal. Chem.* **2011**, *83*, 3770–3777.
(18) Marin, S.; Pujals, S.; Giralt, E.; Merkoci, A. *Bioconjugate Chem.* **2011**, *22*, 180–185.
(19) Wang, D. Y.; Rogach, A. L.; Caruso, F. *Nano Lett.* **2002**, *2*, 857–861.
(20) Qian, J.; Zhang, C. Y.; Cao, X. D.; Liu, S. Q. *Anal. Chem.* **2010**, *82*, 6422–6429.
(21) Xiang, Y.; Zhang, H. X.; Jiang, B. Y.; Chai, Y. Q.; Yuan, R. *Anal. Chem.* **2011**, *83*, 4302–4306.
(22) Tang, Y. F.; Allen, B. L.; Kauffman, D. R.; Star, A. *J. Am. Chem. Soc.* **2009**, *131*, 13200–13201.
(23) Xu, X.; Jiang, S. J.; Hu, Z.; Liu, S. Q. *ACS Nano* **2010**, *4*, 4292–4298.
(24) El-Said, W. A.; Kim, T. H.; Kim, H.; Choi, J. W. *Biosens. Bioelectron.* **2010**, *26*, 1486–1492.
(25) Xu, W.; Xue, X. J.; Li, T. H.; Zeng, H. Q.; Liu, X. G. *Angew. Chem., Int. Ed.* **2009**, *48*, 6849–6852.
(26) Zhang, J. J.; Cheng, F. F.; Zheng, T. T.; Zhu, J. J. *Anal. Chem.* **2010**, *82*, 3547–3555.
(27) Ding, C. F.; Ge, Y.; Zhang, S. S. *Chem.—Eur. J.* **2010**, *16*, 10707–10714.
(28) Cui, R. J.; Pan, H. C.; Zhu, J. J.; Chen, H. Y. *Anal. Chem.* **2007**, *79*, 8494–8501.
(29) Zhang, J. J.; Zheng, T. T.; Cheng, F. F.; Zhu, J. J. *Chem. Commun.* **2011**, *47*, 1178–1180.
(30) Decher, G.; Hong, J. D. *Makromol. Chem., Macromol. Symp.* **1991**, *46*, 321–327.
(31) Quinn, J. F.; Johnston, A. P. R.; Such, G. K.; Zelikin, A. N.; Caruso, F. *Chem. Soc. Rev.* **2007**, *36*, 707–718.
(32) Chen, D.; Wang, G.; Lu, W.; Zhang, H.; Li, J. H. *Electrochem. Commun.* **2007**, *9*, 2151–2156.
(33) Li, J.; Zhao, X. W.; Zhao, Y. J.; Gu, Z. Z. *Chem. Commun.* **2009**, *45*, 2329–2331.
(34) Jin, L. H.; Shang, L.; Zhai, J. F.; Li, J.; Dong, S. J. *J. Phys. Chem. C* **2010**, *114*, 803–807.
(35) Pu, K. Y.; Zhan, R. Y.; Liu, B. *Chem. Commun.* **2010**, *46*, 1470–1472.
(36) Le Gac, S.; Vermes, I.; van den Berg, A. *Nano Lett.* **2006**, *6*, 1863–1869.
(37) Shynkar, V. V.; Klymchenko, A. S.; Kunzelmann, C.; Duportail, G.; Muller, C. D.; Demchenko, A. P.; Freyssinet, J. M.; Mely, Y. *J. Am. Chem. Soc.* **2007**, *129*, 2187–2193.
(38) Savill, J. *Br. Med. Bull.* **1997**, *53*, 491–508.
(39) Rapoport, E.; Le Pendu, J. *Glycobiology* **1999**, *9*, 1337–1345.
(40) Hart, S. P.; Ross, J. A.; Ross, K.; Haslett, C.; Dransfield, I. *Cell Death Differ.* **2000**, *7*, 493–503.
(41) Yan, J.; Hu, M.; Li, D.; He, Y.; Zhao, R.; Jiang, X. Y.; Song, S. P.; Wang, L. H.; Fan, C. H. *Nano Res.* **2008**, *1*, 490–496.
(42) Hu, M.; Yan, J.; He, Y.; Lu, H. T.; Weng, L. X.; Song, S. P.; Fan, C. H.; Wang, L. H. *ACS Nano* **2010**, *4*, 488–494.